Design-Oriented Transient Stability Analysis of Grid-Connected Converters: A Comparative Study of Analysis Methods

Chao Charles Liu, *Graduate Student Member, IEEE*, Chi K. Tse, *Fellow, IEEE*, Meng Huang, *Member, IEEE*, Zhenxi Wu, *Student Member, IEEE*, Hua Han, *Member, IEEE*, and Jingxi Yang, *Member, IEEE*

***Abstract*—Transient stability analysis of grid-connected converters can provide guidance for practical design. Previous studies have summarized monotonic relationships between stability and parameters. Given the complex nonlinear behavior of converter-based systems, these monotonic relationships are incomplete. In this article, design guidelines in the form of feasible parameter ranges are developed. Sensitivity analysis and bifurcation diagrams are utilized to derive feasible parameter ranges from typical stability analysis methods, including time-domain simulation, energy-based methods (manually derived and algorithmically searched), and bifurcation analysis. It is found that different analysis methods may provide equivalent design guidelines due to the similar sensitivity patterns identified by these methods. Furthermore, we reveal that the change in the sensitivity patterns can be induced by the bifurcation behavior of grid-connected converters. Therefore, the qualitative differences between the stability analysis methods are determined by their ability to capture the various bifurcations crucial for determining transient stability. Our results show different levels of consistency between the analysis methods. The findings are verified by laboratory experiments.**

***Index Terms*—Bifurcation analysis, grid-following converter (GFLC), grid-forming converter (GFMC), Lyapunov method, sensitivity analysis, transient stability.**

I. Introduction

As MODERN power systems containing significant number of power electronics converters may encounter large disturbances, the significance of transient stability of grid-connected power converters has gained increasing attention [1], [2]. Recently, a number of dynamical models and analysis tools have been developed to study transient stability. With many physically insightful results obtained, the research on transient stability of grid-connected converters has reached a stage where the focus can be directed from dynamical analysis toward practical design [1], [3]. It is thus of practical importance to evaluate the analysis methods from a design-oriented perspective [4].

The first task of design-oriented transient stability analysis is to establish large-signal models for practical converters with high fidelity. Due to the difficulty of elucidating high-order models, order reduction is commonly applied to simplify analysis [5], [6], [7]. Specifically, the outer synchronization loops of converters are generally preserved, while the inner control loops (e.g., current loops) can be omitted. For instance, the second-order model containing a phase-locked loop (PLL) is widely utilized for studying grid-following converters (GFLCs) [5]. Also, depending on whether a lowpass filter (LPF) is used for noise suppression and inertia emulation, a first-order or second-order model containing a power synchronization loop can be adopted for investigating grid-forming converters (GFMCs) [6], [7]. While such order reduction enables simple and intuitive analysis of instability phenomena of converters, the applicability of the simplified models to practical design is not guaranteed. The findings of recent studies have underlined the importance of the preconditions of using simplified models [8], [9]. Generally, the simplified models should be used only when the internal loops are much faster than the synchronization loops. It is worth noting that tuning of the bandwidth of the inner loops is always necessary, and the applicability of simplified models also depends on the use of power decoupling and feedforward compensation [8].

The next issue is the capability of large-signal models in assessing transient stability. Such capability can be characterized by the basin of attraction (BOA) of a stable equilibrium point (SEP), of which the shape and size primarily affect the stability metrics of converter-based systems. As shown in Fig. 1, typical BOA estimation methods can be classified into three types, in accordance with the preferences of different communities. First, time-domain simulation (TDS), or the phase portrait method, directly computes the transient trajectories via step-by-step numerical integration and thus requires no in-depth understanding of the system's nonlinear behavior [7], [10]. The BOA is estimated

Received 1 August 2024; revised 29 September 2024; accepted 13 October 2024. Date of publication 16 October 2024; date of current version 12 December 2024. This work was supported in part by the Hong Kong Research Grants Council under Grant 112015/24, in part by the City University of Hong Kong under Grant 9229105 and Grant 9380114, and in part by the National Natural Science Foundation of China under Grant 52222707. Recommended for publication by Associate Editor L. Chang. *(Corresponding author: Jingxi Yang.)*

Chao Charles Liu, Chi K. Tse, Zhenxi Wu, and Jingxi Yang are with the Department of Electrical Engineering, City University of Hong Kong, Hong Kong (e-mail: chao.liu@my.cityu.edu.hk; chitse@cityu.edu.hk; zhenxiwu2-c@my.cityu.edu.hk; jyang264@cityu.edu.hk).

Meng Huang is with the School of Electrical Engineering and Automation, Wuhan University, Wuhan 430072, China (e-mail: meng.huang@whu.edu.cn).

Hua Han is with the School of Automation, Central South University, Changsha 410017, China (e-mail: hua_han0523@csu.edu.cn).

Color versions of one or more figures in this article are available at https://doi.org/10.1109/TPEL.2024.3481495.

Digital Object Identifier 10.1109/TPEL.2024.3481495

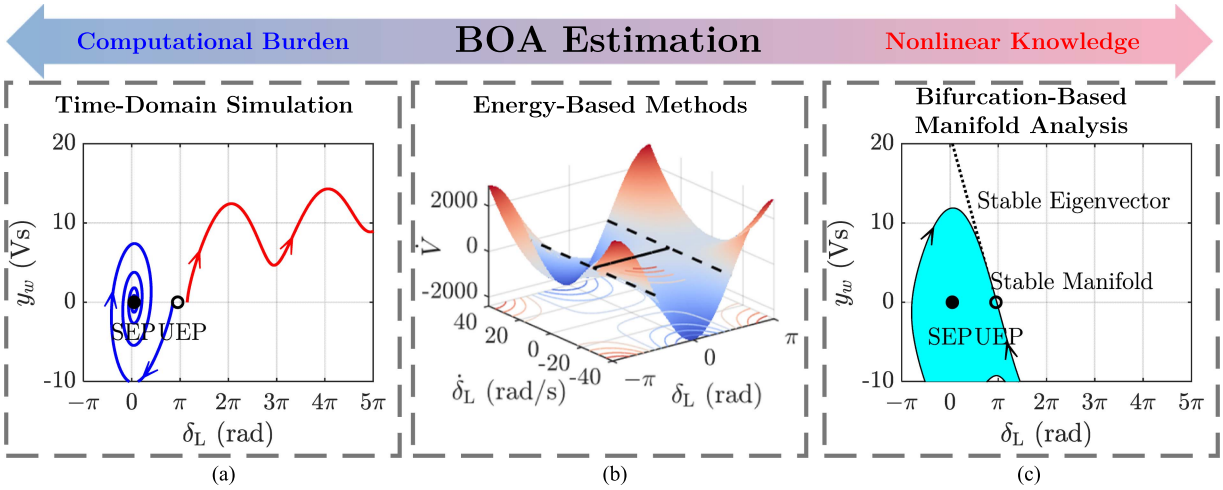

Fig. 1. Examples of BOA estimation methods applied to GFLC with $\kappa_p = 0.1$ p.u. (a) Time-domain simulation; (b) lie derivative of the energy function of the swing equation; (c) bifurcation-based manifold analysis.

by scanning the state space and identifying the convergence or divergence of trajectories. Despite its high computational burden, TDS is mostly adopted by the industry due to its high reliability and broad applicability [2], [11]. However, TDS does not provide sufficient information for developing a systematic design methodology. Second, *energy-based methods* are more appealing due to their better physical intuitions and high analyticity. These methods seek to identify the condition under which the system's equivalent energy contracts monotonically to ensure stability. Based on earlier research on conventional power systems, typical energy-based methods for grid-connected converters include the equal-area criterion (EAC) [12], [13], [14], [15], and Lyapunov's direct method [16], [17], [18], [19]. A major challenge in using energy-based methods is that the results are conservative in nature [11]. Recent advances in convex optimization [18] and machine learning [20] have made it possible to search energy functions with lower levels of conservation via automatic algorithms. However, it is yet to be clarified whether quantitative improvements of energy-based methods can substantially benefit the design of converter-based systems. The third category of methods utlizes *nonlinear studies,* which typically demonstrate the exact BOA boundary of converter-based systems using bifurcation-based manifold analysis [8], [14], [21], [22], [23]. According to Chiang et al. [24], with certain conditions satisfied (which hold in general for converter-based systems), the BOA boundary of a nonlinear system is composed by the union of the stable manifolds of all equilibrium points and periodic orbits on the boundary. Thus, the exact BOA boundary can be obtained by directly computing the relevant manifolds. For simplicity, the estimation can be performed by considering only the stable manifolds of equilibrium points [12]. However, without employing bifurcation analysis, the simplified approach will solely cover a part of all possible operating regimes (i.e., composition of the BOA boundary). With variation of parameters, the composition of the BOA boundary will change due to the emergence or disappearance of periodic orbits. As qualitative changes are affected by the bifurcation behavior of the system, bifurcation-based manifold analysis offers a more comprehensive view of the BOA boundary for guiding the parameter design. Nevertheless, bifurcation analysis involves indepth mathematical analysis of dynamical systems and is considered a relatively complex method.

For the purpose of practical design, many studies have attempted to derive design guidelines concerning transient stability. Most design guidelines, however, focus on monotonic relationships between stability and parameters [7], [10], [12], [16], [17], which may only hold for certain parameter conditions. Determining parameter values through these monotonic relationships still requires practical experience and may encounter contradictions between different stability and response metrics. For instance, increasing the cutoff frequency of the LPF of GFMCs improves transient stability but results in weaker inertia support [19], [25]. On the other hand, direct acquisition of optimal parameter values is challenging due to the difficulty of formulating a solvable optimization problem.

To provide effective design guidelines, we aim to identify *feasible parameter ranges* and leave the final choices to engineers. The results of bifurcation analysis (i.e., bifurcation diagrams) are essentially such type of design guidelines [4]. To derive design guidelines from TDS and energy-based methods, we perform sensitivity analysis on the stability metrics estimated by these methods. The sensitivity analysis provides critical insights into the effects of parameters on transient stability [26].

Despite the quantitative differences in the estimated stability metrics, the analysis methods may give similar sensitivity patterns, leading to equivalent parameter suggestions. By comparing the design guidelines, we reveal the qualitative differences between the various stability analysis methods as well as their practical values for parameter design. Moreover, we apply bifurcation analysis to identify these qualitative differences. This study may thus benefit engineers with diverse backgrounds by presenting advanced analytical methods in a simple yet practical way.

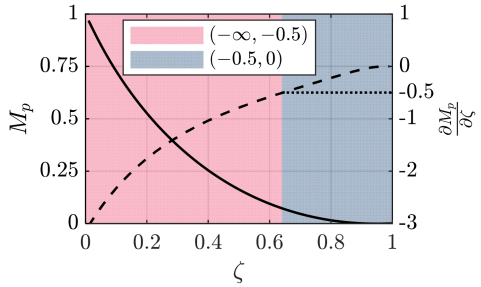

Fig. 2. Overshoot (solid line) and its sensitivity (dashed line) to damping ratio for a standard second-order linear system.

II. Design Methodology

A. Sensitivity Analysis

The sensitivity of performance metrics provides insightful information for tuning control parameters, especially for scenarios with necessary tradeoffs. Even for a linear system (i.e., with a linear relationship between input, state, and output), the relationship between the sensitivity of performance metrics and parameters is nonlinear in general, which signifies the varying influences of parameters with the change of parameter choices.

For example, Fig. 2 shows the sensitivity of overshoot M_p to damping ratio ζ for a standard second-order linear system [27]. The negative sensitivity suggests increasing ζ to reduce M_p. However, as ζ approaches 1, the sensitivity of M_p decreases slowly to zero, indicating a diminishing marginal return. Also, increasing ζ up to 1 will result in longer settling time (peak time). Considering the tradeoff between overshoot and response speed, a damping ratio slightly smaller than 1 (e.g., $1/\sqrt{2}$) is widely adopted. The above-mentioned analysis can be summarized as a design guideline by dividing the whole parameter range into two subranges with contrasting sensitivities, of which the one with small overshoot and low sensitivity is recommended. Specifically, we can choose ζ in (0.64,1) to have a sensitivity lower than 0.5 in absolute value, as highlighted in blue in Fig. 2. Eventually, a relatively small damping ratio in the low-sensitivity range enables a small overshoot and fast response simultaneously.

The varying influence of parameters becomes more significant in grid-connected converters, where the nonlinear behavior can lead to nonsmooth and extremely contrasting sensitivity patterns. For example, the response of GFLCs against consecutive voltage dips is presented in Fig. 3 to show the sensitivity of the critical clearing time t_c to the proportional control parameter κ_p. The response is obtained via full-circuit simulation on MATLAB/Simulink. As shown in Fig. 3(a), the GFLC with $\kappa_p = 0.1$ p.u. recovers stability after a fault lasting for 0.12 s, but loses synchronization as the fault duration increases to 0.14 s. Thus, the converter's critical clearing time (i.e., maximum endurable fault duration) is about 0.13 s. For the case in Fig. 3(b), choosing κ_p of 0.2 p.u. leads to the same t_c of about 0.13 s, indicating a low sensitivity between κ_p of 0.1 and 0.2 p.u. However, when κ_p increases from 0.2 to 0.22 p.u, the critical clearing time nearly doubles, implying a very high sensitivity. Such contrasting results underline the importance of considering the varying influence of parameters on transient stability.

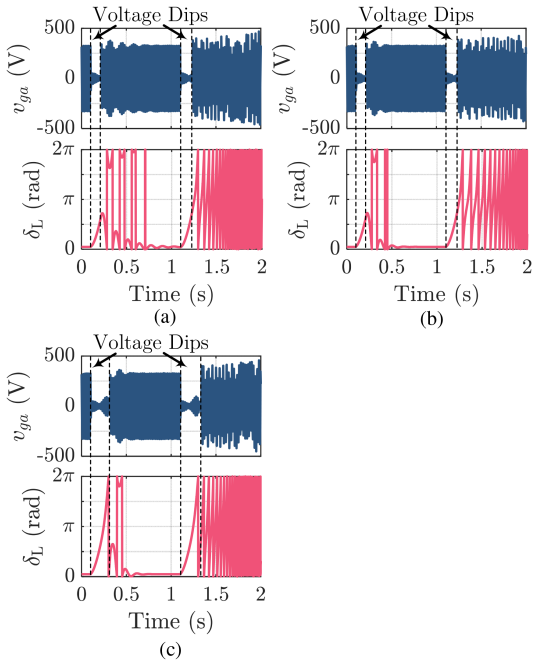

Fig. 3. Full-circuit simulation of GFLC with consecutive voltage dips. (a) $\kappa_p = 0.1$ p.u. and fault lasting for 0.12 s and 0.14 s; (b) $\kappa_p = 0.2$ p.u. and fault lasting for 0.12 s and 0.14 s; (c) $\kappa_p = 0.22$ p.u. and fault lasting for 0.22 s and 0.24 s.

While the primary role of sensitivity analysis in our design-oriented analysis is to improve stability metrics, the estimated sensitivity also facilitates other design considerations. Our previous studies have identified exhibiting low or zero sensitivity in relatively long parameter ranges as a common property of grid-connected converters [8], [21], [22]. The low sensitivity enables us to improve other metrics without resulting in severe stability degradation. For example, the GFMC can achieve a satisfactory tradeoff between transient stability and inertia support by choosing a relatively low cutoff frequency in the low-sensitivity range [21]. Besides, the sensitivity analysis also benefits the robustness of the design against parameter variations. Due to the nonlinear behavior of converters, the low sensitivity to controllable parameters (e.g., controller parameters) and uncontrollable parameters (e.g., grid impedance) can be realized simultaneously. Thanks to these properties, we are able to derive practical design guidelines by applying sensitivity analysis.

Another method to obtain feasible parameter ranges is to specify the minimum requirement of performance metrics [7], [10], [19]. This requirement-based method can provide equivalent parameter suggestions to the sensitivity-based method when the minimum requirement is appropriately defined. However, like applying the monotonic relationships, determining the minimum requirement of performance metrics still relies on engineering experience and may result in trivial or unfeasible solutions. The requirement-based and sensitivity-based methods will be compared in Section V-E.

B. Design Framework

The basic framework for design-oriented transient stability analysis is presented in Fig. 4. Before conducting transient

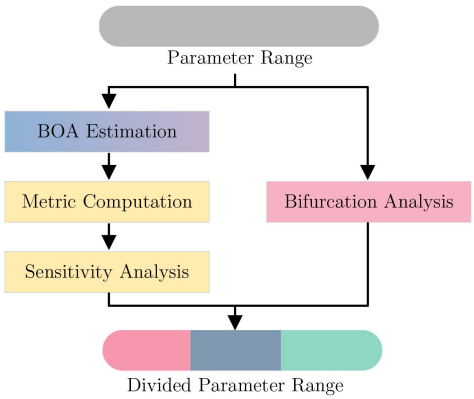

Fig. 4. Design framework.

stability analysis, an initial design should be obtained via small-signal stability analysis. Then, the dominating parameters for transient stability are chosen for sensitivity analysis. Since the simplified models of grid-connected converters are generally second order [5], [7], two parameters at most need to be tuned. For each of the BOA estimation methods, the BOA under parameter changes is estimated to compute the concerned stability metrics and their sensitivity to parameters. Finally, the parameter ranges are divided into several subranges with distinct sensitivity patterns, and the one with high stability metrics and low sensitivity is chosen as the recommended feasible parameter range.

We apply the above-mentioned procedure to TDS and energy-based methods but not bifurcation analysis. This is due to the fact that the BOA estimates of bifurcation-based manifold analysis are the same as those of TDS. Moreover, the bifurcation diagrams obtained from bifurcation analysis directly divide the parameter space using bifurcation boundaries. The bifurcation boundaries are defined from the perspective of different operating regimes (topological equivalence of phase portraits in studies of dynamical systems [28]) [4]. The parameter range of the expected operating regime provides a design guideline for bifurcation analysis. We will examine the two types of design guidelines in Section V-C.

III. Large-Signal Models

A grid-connected power converter includes a power stage and a filter connected to the power grid, as shown in Fig. 5. This article focuses on two types of grid-connected converters due to their relatively mature applications, namely, GFLCs using a synchronous-reference-frame PLL and GFMCs employing P-f droop control. Among other typical grid-forming control methods, power synchronization control [6] and virtual synchronous generators control [7] are equivalent to the studied droop control, while virtual oscillator control exhibits distinct time-domain dynamics [29] and will be studied in future work.

The power grid is modeled as a stiff voltage source and a grid impedance. The magnitude and phase angle of the stiff source are denoted by V_{sm} and θ_s, respectively. To indicate the different grid-strength compatibility, we denote the inductance of the grid impedance for the GFLC and GFMC by L_s and L_l, respectively.

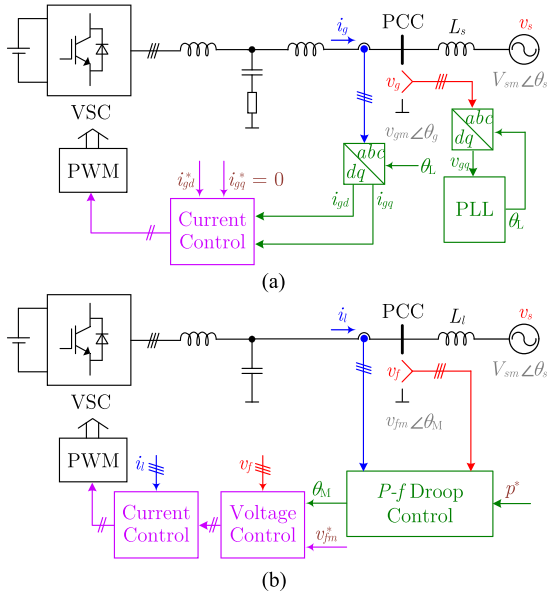

Fig. 5. Circuits and control structures of (a) GFLC and (b) GFMC.

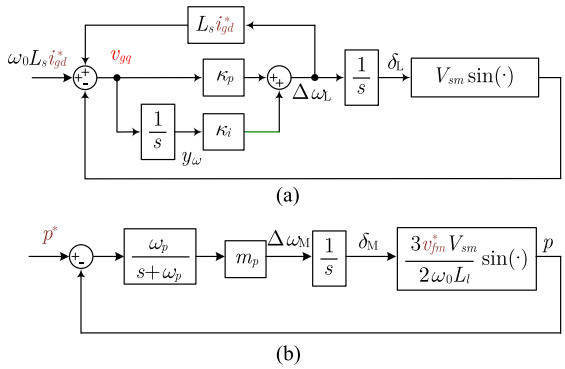

Fig. 6. Large-signal models of (a) GFLC and (b) GFMC.

While the GFMC here adopts the alternating-voltage control, our analysis can be flexibly extended to those with a Q-V droop control [7], [21].

We assume that the inner control loops feature high bandwidth, power decoupling, and feedforward compensation such that their transient process can be omitted in the time-scale of the outer synchronization loops [8]. Hence, we obtain the large-signal models shown in Fig. 6 by approximating the inner control loops as unity-gain loops.

The dynamics of a GFLC are described by

$$\begin{cases} \dot{y}_\omega = -V_{sm}\sin\delta_{\rm L} + L_s i_{gd}^* \dfrac{-\kappa_p V_{sm}\sin\delta_{\rm L}+\kappa_i y_\omega+\omega_0}{1-\kappa_p L_s i_{gd}^*} \\ \dot{\delta}_{\rm L} = \dfrac{-\kappa_p V_{sm}\sin\delta_{\rm L}+\kappa_i y_\omega+\omega_0}{1-\kappa_p L_s i_{gd}^*} - \omega_0 \end{cases} \tag{1}$$

where y_ω is the state variable of the PLL controller, $\delta_{\rm L} = \theta_{\rm L} - \theta_s$ is the phase difference, i_{gd}^* is the current reference for active power, ω_0 is the operating frequency of the grid, and κ_p and κ_i are the proportional and integral gains, respectively.

TABLE I
DEFAULT PARAMETERS OF GFLCS

Parameter	Value	p.u.	Parameter	Value	p.u.
V_{sm}	311 V	1	i^*_{gd}	30 A	1
L_s	5 mH	0.152	κ_p	0.413	1
ω_0	100π rad/s	1	κ_i	7.786	1

The GFMC is modeled as

$$\begin{cases} \Delta\dot{\omega}_{\mathrm{M}} = \omega_p \left(-\Delta\omega_{\mathrm{M}} - m_p \frac{3v^*_{fm} V_{sm} \sin\delta_{\mathrm{M}}}{2\omega_0 L_l} + m_p p^* \right) \\ \dot{\delta}_{\mathrm{M}} = \Delta\omega_{\mathrm{M}} \end{cases} \tag{2}$$

where $\Delta\omega_{\mathrm{M}}$ is the frequency difference between the GFMC and the grid, ω_p is the cutoff frequency of the LPF, m_p is the droop gain, v^*_{fm} is the reference of the voltage magnitude, $\delta_{\mathrm{M}} = \theta_{\mathrm{M}} - \theta_s$ is the phase difference, and p^* is the power reference.

In applying energy-based methods, the models of (1) and (2) are usually transformed into the form of swing equations [11] by establishing an analogy between converters and synchronous generators. The swing equation is represented as

$$J\ddot{\delta} = P_m - P_e - D\dot{\delta} \tag{3}$$

where J is the equivalent moment of inertia, P_m is the equivalent mechanical power, P_e is the equivalent electromagnetic power, and D is the equivalent damping coefficient.

For the GFLC, the equivalent representation is obtained as

$$\begin{cases} \delta = \delta_{\mathrm{L}} \\ J = \frac{1-\kappa_p L_s i^*_{gd}}{\kappa_i} \\ P_m = \omega_0 L_s i^*_{gd} \\ P_e = V_{sm} \sin\delta_{\mathrm{L}} \\ D = \frac{\kappa_p}{\kappa_i} V_{sm} \cos\delta_{\mathrm{L}} - L_s i^*_{gd}. \end{cases} \tag{4}$$

Likewise, the swing equation of the GFMC is derived by

$$\begin{cases} \delta = \delta_{\mathrm{M}} \\ J = \frac{1}{\omega_p m_p} \\ P_m = p^* \\ P_e = \frac{3v^*_{fm} V_{sm} \sin\delta_{\mathrm{M}}}{2\omega_0 L_l} \\ D = \frac{1}{m_p}. \end{cases} \tag{5}$$

It should be noted that although the models of (1) and (3)–(4) are equivalent, they may produce different responses in face of grid disturbances. For example, when a phase jump or voltage dip occurs, y_ω in (1) remains zero at the instant of the disturbance, but $\dot{\delta}_{\mathrm{L}}$ will suffer from a sudden change due to the proportional gain of the PLL controller. In comparison, following the tradition of synchronous generators, the model of (3) assumes $\dot{\delta}$ to be zero at the instant of the disturbance, which is common in EAC analysis [12], [13], [14], [15]. To reduce error, an additional state jump should be considered when the model of (3) is applied.

Throughout the analysis in this article, the default parameters in Tables I and II are adopted, unless otherwise stated. By default, the GFLC and GFMC are designed to operate at 14 and 25 kW, respectively.

TABLE II
DEFAULT PARAMETERS OF GFMCS

Parameter	Value	p.u.	Parameter	Value	p.u.
V_{sm}	311 V	1	p^*	25 kW	1
L_l	15 mH	0.812	ω_p	$2\pi \times 0.1$	0.1
ω_0	100π rad/s	1	m_p	$\frac{0.02\omega_0}{P_{\max}}$	0.02
v^*_{fm}	311 V	1			

Note: $P_{\max}$ is the maximum injection power and chosen as p^* in this article.

TABLE III
ENERGY-BASED METHODS

Method	Advantage	Limitation
EAC	Simple	Damping assumed
Energy function of swing equation	Intuitive	Conservative
SOSP	Less conservative	Numerical error
LNN	Formal and rigorous	Less efficient

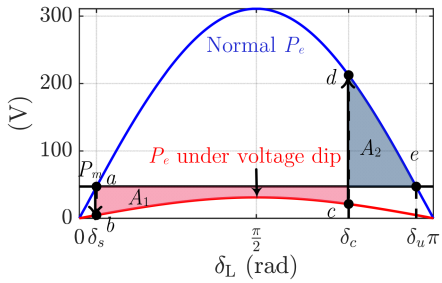

Fig. 7. EAC for GFLC suffering from a voltage dip with $V^f_{sm} = 0.1$ p.u.

IV. ANALYSIS METHODS OF TRANSIENT STABILITY

This section presents the typical transient stability analysis methods. As introduced in Section I, TDS has been commonly used for transient stability analysis. The classical Runge–Kutta method [11] can solve the low-order models in (1) and (2) with very high accuracy, which will be omitted in this article. Moreover, we will present the salient concepts with minimal technical details to facilitate easy grasp of the essential differences of the various methods.

A. Energy-Based Methods

In this article, we consider four typical energy-based methods, as shown in Table III. EAC considers the equivalent motion of the swing equation [11], [12]. Fig. 7 shows an example of a GFLC suffering from a voltage dip, where δ_s and δ_u are the phase differences at the SEP and the unstable equilibrium point (UEP), respectively. Similar grid disturbances will create an imbalance between P_m and P_e, and subsequently cause the acceleration or deceleration of the equivalent motion of (3). The equivalent energy change is characterized by an accelerating area A_1 and a maximum decelerating area A_2. The converter-based systems are judged as stable when disturbances are cleared before the critical clearing angle δ_c, where $A_1 = A_2$. Finally, the critical clearing angle is translated to the critical clearing time t_c using trajectories computed from TDS.

Assuming positive damping, the analysis of EAC implies a Lyapunov function composed of potential energy and kinetic energy [11], [17]. The potential energy is

$$E_p = -\int_{\delta_s}^{\delta} (P_m - P_e(u))du \tag{6}$$

where u denotes the variable of integration for δ. The kinetic energy is

$$E_k = \frac{1}{2} J\dot{\delta}^2. \tag{7}$$

Thus, the energy (Lyapunov) function of grid-connected converters is obtained as

$$V = E_p + E_k \tag{8}$$

with the Lie derivative given as

$$\dot{V} = \frac{\partial V}{\partial \boldsymbol{x}} \frac{\partial \boldsymbol{x}}{\partial t} = -D\dot{\delta}^2 \tag{9}$$

where $\boldsymbol{x} = [\delta\ \dot{\delta}]^{\mathrm{T}}$ is the state vector. The energy function given in (8) can be used to estimate the SEP's BOA via La Salle's invariance principle [17]. In short, the BOA is identified as the connected component of a sublevel set $\bar{\Omega}_c = \{\boldsymbol{x} : V(\boldsymbol{x}) \leq c\}$, where $\dot{V}$ is negative semidefinite (i.e., positive damping D) and the SEP is the only included equilibrium point. An example of the Lie derivative for the GFLC is shown in Fig. 1(b), where the area with a negative semidefinite Lie derivative is depicted by dashed lines.

While such manually derived Lyapunov functions provide insightful physical intuitions, their BOA estimates can be too conservative. To improve the accuracy of the estimates, researchers have proposed specific algorithms to search valid candidates of Lyapunov functions [20], [30]. With the state vector $\boldsymbol{x}$ normalized as $\boldsymbol{z}$, the maximization of the BOA estimate involves a sublevel set $\Omega_c = \{\boldsymbol{z} : V(\boldsymbol{z}) \leq c, \dot{V}(\boldsymbol{z}) < 0\}$ and a domain $\mathbb{D} = \{\boldsymbol{z} : \eta(\boldsymbol{z}) < \beta, \dot{V}(\boldsymbol{z}) < 0\}$, where $\eta(\boldsymbol{z})$ is positive-definite and often initialized in the form of $\eta(\boldsymbol{z}) = \sum_i z_i^2$. Depending on the inclusion relationship between Ω_c and $\mathbb{D}$, the problem formulation can be classified into the expanding interior algorithm and expanding domain algorithm [31], as shown in Fig. 8. For both algorithms, the area of $\mathbb{D}$ is enlarged by maximizing β. Hence, a limitation of the expanding domain algorithm is that a large area of $\mathbb{D}$ does not ensure a large area of Ω_c, i.e., the estimated BOA.

To illustrate the expanding interior algorithm and expanding domain algorithm, we implement sum-of-squares programming (SOSP) and Lyapunov neural network (LNN), respectively. In Lyapunov's direct method, the asymptotic stability is determined by positive (negative) semidefiniteness conditions, which are relaxed to a sum-of-squares polynomial in SOSP (feasible space being constrained). Thus, the problem of searching for a valid Lyapunov function is transformed into a convex problem that can be efficiently solved via semidefinite programming. Nevertheless, maximizing the BOA of the found Lyapunov function is a nonconvex problem and can have different heuristic formulations [31]. Our implementation mainly adopts the formulation of Zhang et al. [18] and the solver in SOSTOOLS [32].

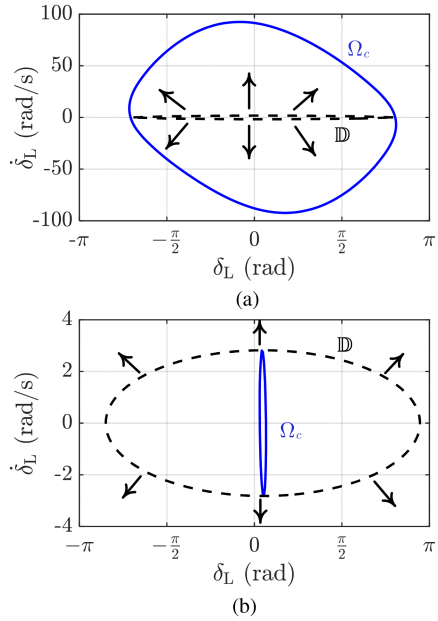

Fig. 8. BOA estimates for GFLC with $\kappa_p = 0.1$ p.u. (a) Expanding interior algorithm implemented by SOSP; (b) expanding domain algorithm implemented by LNN.

While SOSP is relatively mature, it may result in problematic estimates due to numerical errors. To ensure relevance of the estimates, researchers have introduced formal verification into the search of Lyapunov functions. LNN is a representative method that incorporates numerical search and formal verification [20]. This method generally adopts the expanding domain algorithm, as shown in Fig. 8(b). The strict negative-definiteness of $\dot{V}(\boldsymbol{z})$ in $\mathbb{D}$ is ensured by *satisfiability modulo theory* solvers, which also limits computation efficiency. In this article, an open-source toolbox FOSSIL [33] is utilized to search LNNs for grid-connected converters.

B. Bifurcation Analysis

Bifurcation analysis deals with the change of operating regimes of grid-connected converters under parameter variations [4]. The operating regimes can be differentiated by the qualitative difference (topological equivalence) of phase portraits [28]. The purpose of bifurcation analysis is to identify the parameter boundary for the expected operating regime. Early studies on dc/dc converters often define the expected operating regime by the stability of the operating equilibrium point [4]. Such a definition has been extended to small-signal stability studies of ac converter-based systems [34]. However, the problem of transient stability concerns state trajectories escaping from the BOA instead of the loss of the stability of equilibrium points. Consequently, we can have a more flexible definition of the expected operating regime for studying transient stability. In this article, we propose two basic criteria for defining the expected operating regime concerning transient stability.

1) *Large BOA:* The phase portrait should provide a relatively large BOA in the expected operating regime.

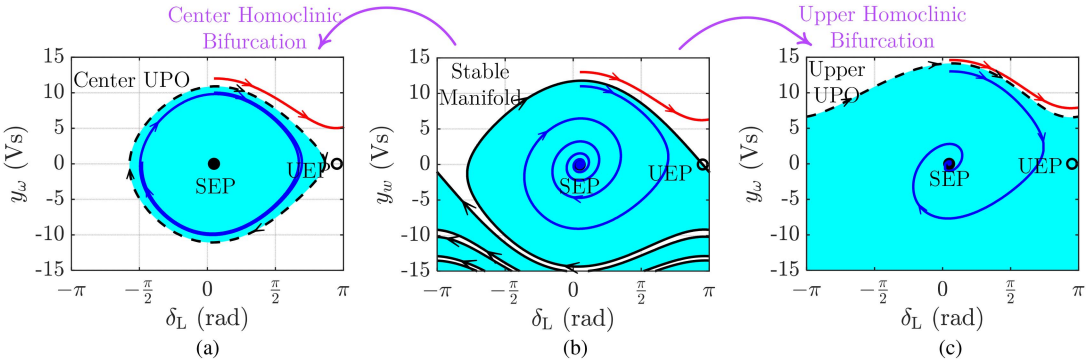

Fig. 9. Phase portraits of GFLC with (a) $\kappa_p = 0.018$ p.u., (b) $\kappa_p = 0.1$ p.u., and (c) $\kappa_p = 0.25$ p.u.

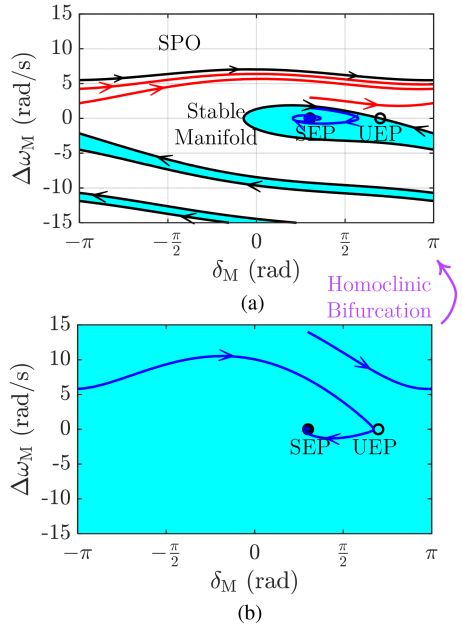

Fig. 10. Phase portraits of GFMC with (a) $\omega_p = 0.1$ p.u. and (b) $\omega_p = 0.7$ p.u.

2) *Low sensitivity:* The sensitivity of stability metrics to parameters should be relatively low under the expected operating regime.

The above-mentioned criteria are applied to study the bifurcation behavior of GFLCs and GFMCs. Our previous studies have revealed the distinct homoclinic bifurcation behavior of these converters [22]. As shown in Fig. 9, GFLCs have three types of phase portraits concerning transient stability, of which the transformation is induced by two homoclinic bifurcations that generate two unstable periodic orbits (UPOs) [8], [14], [22]. In comparison, GFMCs have two types of phase portraits [21], as shown in Fig. 10. Notably, the homoclinic bifurcation of GFMCs generates a stable periodic orbit (SPO) and thus breaks global stability. Comparing the BOA in different phase portraits, we choose those in Figs. 9(c) and 10(b) as the expected operating regimes. While the global stability of GFMCs implies zero sensitivity, the sensitivity of GFLCs will be examined by TDS. Finally, the corresponding bifurcation boundaries in the parameter space, i.e., bifurcation diagrams, are computed to guide the control design. Direct integration [21] or numerical continuation [8] can be employed to perform the computation. Moreover, checking the crossing-UEP resynchronization [22] can represent a simple approach to identifying homoclinic bifurcation of grid-connected converters. For details of the mechanism of homoclinic bifurcation, please refer to Kuznetsov's [28] work.

V. Design-Oriented Analysis

We choose the critical phase jump $\Delta\theta_s$ and the critical clearing time t_c to illustrate the stability metrics of grid-connected converters. The critical phase jump $\Delta\theta_s$ is the maximum phase jump of the grid voltage that converters remain stable. The critical clearing time t_c is the maximum duration of voltage dips that converters can recover synchronization after the faults are cleared. Generally, the two metrics are computed by identifying the marginal cases when the during-fault trajectory touches the boundary of the postfault BOA [11]. Considering that $\Delta\theta_s$ in the negative direction is trapped in the UEP for a relatively long parameter range, as shown in Figs. 9(b) and 10(a), we mainly study positive $\Delta\theta_s$. While $\Delta\theta_s$ is fully determined by the BOA's horizontal axis (δ_L or δ_M), t_c is also affected by the direction and speed of the during-fault trajectory. The EAC analysis indicates that a voltage dip will drive the trajectory to diverge toward the upper right state plane. Hence, the BOA's vertical axis (y_ω or $\Delta\omega_M$) has a significant influence on t_c.

A. Estimation of BOA

To have an intuitive understanding of the difference between analysis methods, we present representative examples of BOA estimation. As shown in Fig. 11, the energy-based methods are conservative for GFLCs in most cases. However, SOSP can give optimistic estimates due to its numerical error, as shown in Fig. 11(c). The increase of κ_p leads to the BOA's connection in line $y_\omega = 0$, making the GFLC robust against any phase jump (i.e., infinite $\Delta\theta_s$). However, such significant robustness enhancement is only captured by TDS and SOSP, as shown in Fig. 11(c). On the other hand, the UEP is included in the estimated BOA boundaries of EAC and SOSP for a relatively large κ_p. Thus, their BOA estimates cover merely a relatively

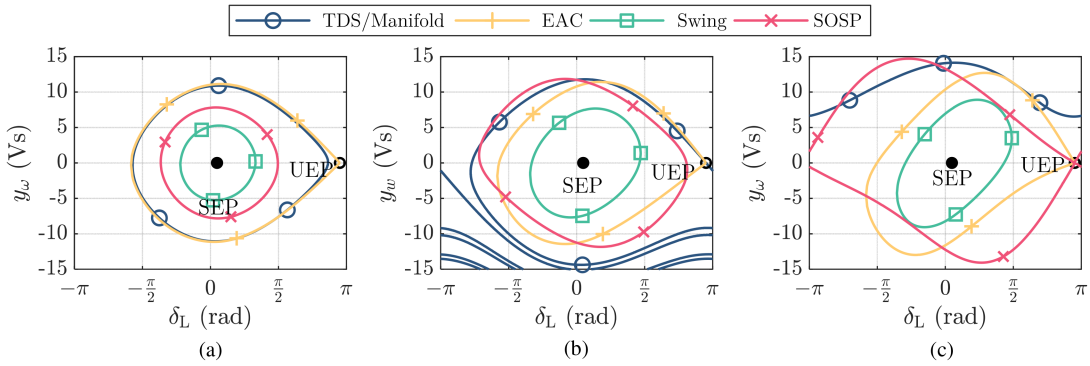

Fig. 11. BOA estimates of GFLC with (a) $\kappa_p = 0.018$ p.u, (b) $\kappa_p = 0.1$ p.u., and (c) $\kappa_p = 0.25$ p.u.

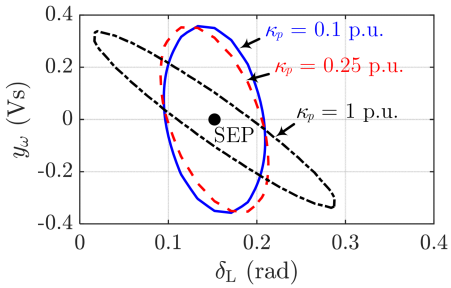

Fig. 12. BOA of GFLC estimated by LNN.

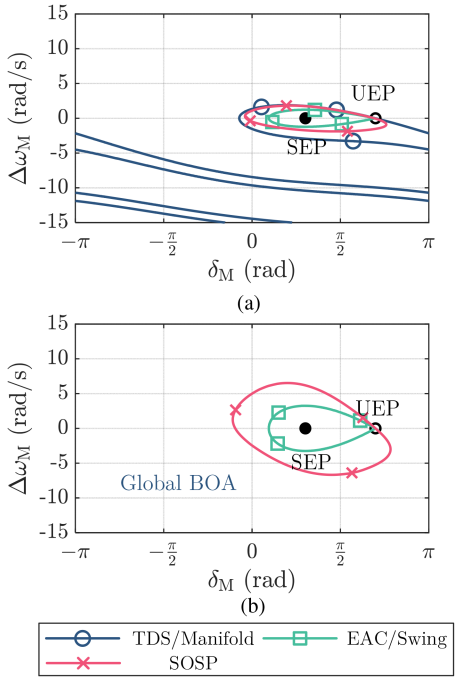

Fig. 13. BOA estimates of GFMC with (a) $\omega_p = 0.1$ p.u. and (b) $\omega_p = 0.7$ p.u.

small part of the upper right state plane, resulting in smaller t_c estimates.

Besides, the BOA estimates of LNNs are shown in Fig. 12. While LNNs ensure the correctness of Lyapunov functions by formal verification, their BOA estimates are very small and are less affected by the change of parameters. A possible reason is the limitation of the expanding domain algorithm, which has been explained in Section IV-A. Changing to the expanding interior algorithm may help improve the BOA estimates of LNNs but will also make it more difficult to perform formal verification. Due to their limited performance, LNN methods are omitted in the following analysis.

Unlike the GFLC, the GFMC has a constant positive damping coefficient D. Consequently, EAC and the energy function of the swing equation are equivalent for the GFMC (with BOA boundaries at the UEP) [17]. As Fig. 13 shows, the increase of the size of BOA with a larger ω_p is captured by EAC and SOSP. However, due to the presence of a UEP, neither method is able to identify the global stability of the GFMC.

B. Sensitivity-Based Design Guidelines

To obtain feasible parameter ranges, we apply the procedure given in Fig. 4 in the transient stability analysis methods. The critical phase jumps of a GFLC with varying κ_p are presented in Fig. 14. From the results of TDS, a very large positive sensitivity is observed near small-signal instability (κ_p smaller than 0.02 p.u.). Then, the sensitivity drops below 15 and remains for a relatively wide range. After an impulse is applied at $\kappa_p = 0.165$ p.u., the sensitivity drops to zero while the GFLC becomes robust to any phase jump. To increase $\Delta\theta_s$ and ensure the design's robustness, we should choose κ_p larger than 0.165 p.u., which is exactly the recommended feasible parameter range of TDS.

Similarly, the sensitivity patterns of all analysis methods are summarized in Fig. 15. Despite the quantitative difference, SOSP captures the three qualitatively different sensitivity patterns revealed by TDS. Thus, the parameter suggestions to increase $\Delta\theta_s$ should be very close for SOSP and TDS. The three sensitivity patterns are also identified by the energy function of the swing equation. However, the energy function has an additional parameter range with negative sensitivity, leading to parameter suggestions with smaller κ_p. Besides, the estimate of EAC remains constant for the whole parameter range, providing little information for improving $\Delta\theta_s$.

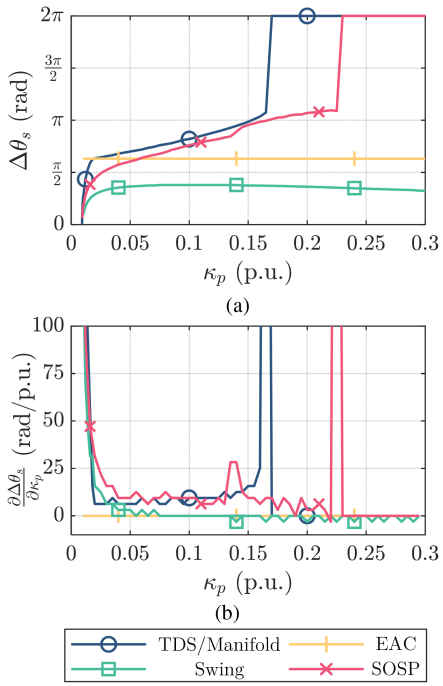

Fig. 14. (a) Critical phase jumps of GFLC; (b) sensitivity to κ_p.

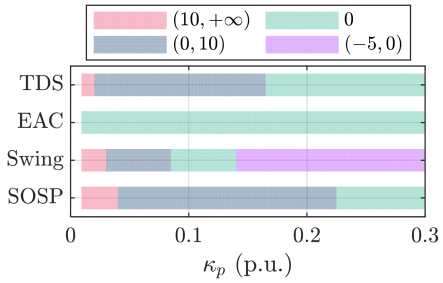

Fig. 15. Parameter range divided by sensitivity patterns of $\Delta\theta_s$ for GFLC.

TABLE IV
DESIGN GUIDELINES FOR GFLC CONCERNING $\Delta\theta_s$

Method	Feasible range κ_p (p.u.)	Sensitivity (rad/p.u.)
TDS	$(0.165, 1)$	$\{0\}$
EAC	$(0.0092, 1)$	$\{0\}$
Swing	$(0.085, 0.14)$	$\{0\}$
SOSP	$(0.225, 1)$	$\{0\}$

By choosing the parameter range with large $\Delta\theta_s$ and low sensitivity, we derive the design guidelines given in Table IV. Specifically, the feasible ranges of TDS and SOSP are chosen as parameter ranges in Fig. 15 with $\Delta\theta_s$ of 2π and zero sensitivity. In comparison, the energy function recommends κ_p to be smaller than 0.14 p.u. due to its negative sensitivity, and EAC does not reflect the impact of κ_p. The results indicate that SOSP is the only energy-based method that provides an equivalent design guideline to TDS. Therefore, concerning the value for design, Lyapunov functions searched via SOSP realize qualitative improvement over the manually derived Lyapunov functions.

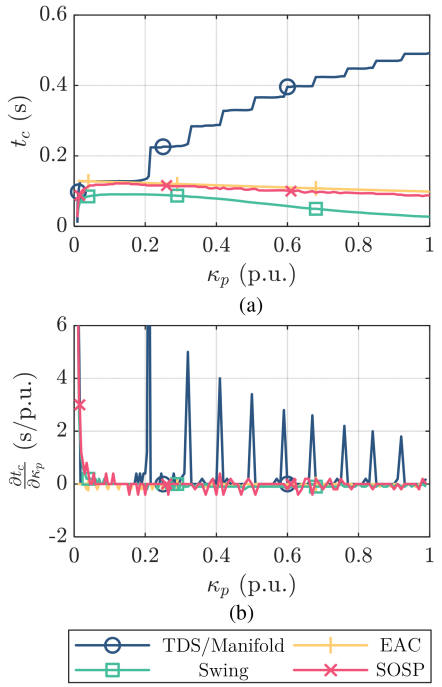

Fig. 16. (a) Critical clearing time of GFLC following a voltage dip with $V_{sm}^f = 0.1$ p.u; (b) sensitivity to κ_p.

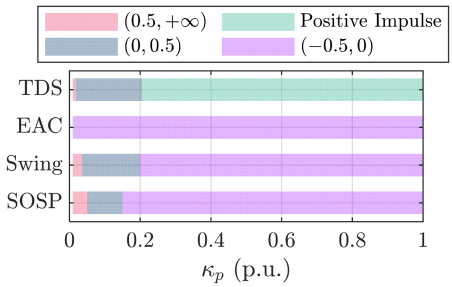

Fig. 17. Parameter range divided by sensitivity patterns of t_c for GFLC.

Next, we perform a design-oriented analysis on the critical clearing time of the GFLC, which depends more on the upper right BOA. Fig. 16 presents the critical clearing time following a voltage dip with during-fault voltage $V_{sm}^f = 0.1$ p.u. The result of TDS indicates a significant difference between $\Delta\theta_s$ and t_c: the zero-sensitivity range of $\Delta\theta_s$ is replaced by an impulse-sensitivity (multiswing resynchronization) range of t_c. This is because the further increase of κ_p will steer the upper UPO, as shown in Fig. 9(c), to move upward, leading to a BOA's extension along the y_ω-axis.

However, the energy-based methods fail to capture the impulse sensitivity pattern, and produce negative sensitivity for κ_p larger than 0.2 p.u. This phenomenon is especially significant for EAC, which holds negative sensitivity for the whole parameter range. As shown in Fig. 17, concerning the critical clearing time, SOSP and the energy function of the swing equation have equivalent sensitivity patterns. Therefore, the two methods suggest very close parameter ranges, as given in Table V. The

TABLE V
DESIGN GUIDELINES FOR GFLC CONCERNING t_c

Method	Feasible range κ_p (p.u.)	Sensitivity (rad/p.u.)
TDS	$(0.205, 1)$	Positive impulse
EAC	$(0.0092, 1)$	$(-0.5, 0)$
Swing	$(0.035, 0.2)$	$(0, 0.5)$
SOSP	$(0.05, 0.15)$	$(0, 0.5)$

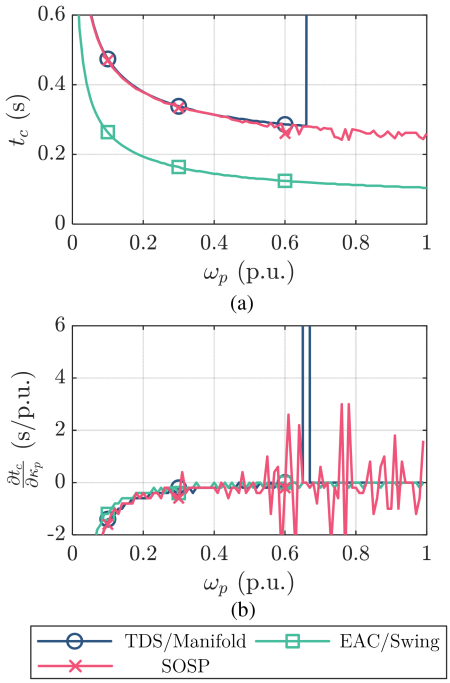

Fig. 18. (a) Critical clearing time of GFMC following a voltage dip with $V_{sm}^f = 0.1$ p.u; (b) sensitivity to ω_p.

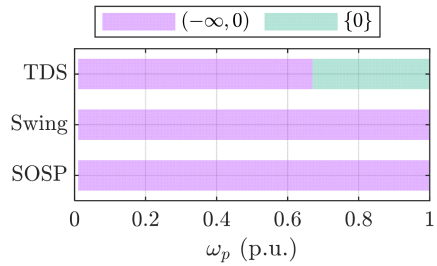

Fig. 19. Parameter range divided by sensitivity patterns of t_c for GFMC.

TABLE VI
DESIGN GUIDELINES FOR GFMC CONCERNING t_c

Method	Feasible range ω_p (p.u.)	Sensitivity (rad/p.u.)
TDS	$(0.67, 1)$	$\{0\}$
Swing	$(0.01, 1)$	$(-\infty, 0)$
SOSP	$(0.01, 1)$	$(-\infty, 0)$

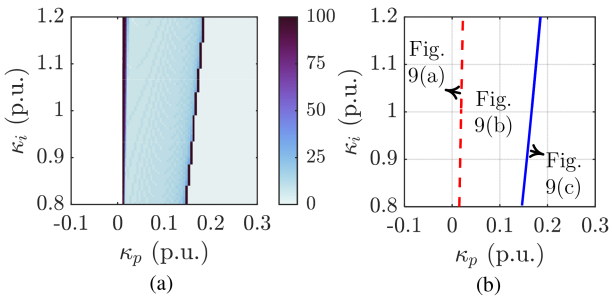

Fig. 20. (a) $\frac{\partial \Delta\theta_s}{\partial \kappa_p}$ of GFLC computed by TDS; (b) bifurcation diagram in the (κ_p, κ_i)-plane. For clarity, sensitivity above 100 is reduced to 100, and the center and upper homoclinic bifurcations are denoted by dashed and solid lines, respectively.

analysis of the critical clearing time indicates a qualitative gap between energy-based methods and TDS for guiding the control design.

To further demonstrate the sensitivity-based design guideline, we investigate the critical clearing time of the GFMC. As shown in Fig. 18, all considered methods capture the decrease of t_c with the increase of ω_p under relatively small ω_p. However, in the result of TDS, t_c jumps to infinity at $\omega_p = 0.67$ p.u. In contrast, t_c estimated by the energy-based methods continue to decrease. Although SOSP exhibits oscillating sensitivity under relatively large ω_p, the sensitivity can be considered negative after the process of moving average. Moreover, choosing parameters in the low-sensitivity ranges of energy-based methods will sacrifice t_c estimates, which implies a conflict between the performance metric and the robustness against parameter variations. From the sensitivity patterns shown in Fig. 19, we derive the design guidelines from these methods, which are given in Table VI. The result indicates a significant difference between the design guidelines not only in the range but also in the trend. Specifically, TDS suggests a relatively large ω_p. To understand this phenomenon, we recognize that an infinite ω_p will render a second-order GFMC [7] equivalent to a first-order GFMC [6] that can resynchronize as long as a SEP exists. In comparison, without capturing the global stability under a relatively large ω_p, the energy-based methods recommend a smaller ω_p such that the diverging speed of the during-fault trajectory is reduced.

In summary, the sensitivity analysis of the two types of converters indicates that the energy-based methods capture parts of the sensitivity patterns as revealed by TDS. This partial consistency leads to a qualitative difference in the corresponding design guidelines. Therefore, from a design-oriented perspective, the results of energy-based methods should be examined and improved by TDS. This observation is consistent with the previous conclusions on traditional power systems [11].

On the other hand, there may be a dynamical origin for the common sensitivity patterns and the corresponding design guidelines. This important characteristic of grid-connected converters is explained in the following section in the light of bifurcation analysis.

C. Consistency With Bifurcation Analysis

To derive the design guidelines from bifurcation analysis, we compute bifurcation diagrams using numerical continuation. Fig. 20(b) shows the bifurcation diagram of a GFLC, where the (κ_p, κ_i)-plane is divided by two homoclinic bifurcations

TABLE VII
BIFURCATIONS EMBODIED BY DESIGN GUIDELINES OF GFLCS

Bifurcation	Center homoclinic	Upper homoclinic
Method	Swing and SOSP (t_c)	TDS and SOSP ($\Delta\theta_s$)

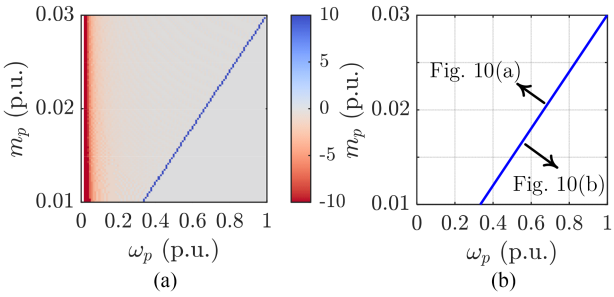

Fig. 21. (a) $\frac{\partial t_c}{\partial \omega_p}$ of GFMC computed by TDS; (b) bifurcation diagram in the (ω_p, m_p)-plane. For clarity, the absolute value of the sensitivity above 10 is reduced to 10.

into three areas with qualitatively different phase portraits. The expected operating regime is at the right-hand side of the upper homoclinic bifurcation. Besides, we analyze the sensitivity of $\Delta\theta_s$ through TDS, which is presented in Fig. 20(a). The result of TDS suggests parameters in the range with infinite $\Delta\theta_s$ and zero sensitivity, which is exactly at the bottom-right side of the upper homoclinic bifurcation. The results indicate that the boundaries of sensitivity-based guidelines can embody bifurcations relevant to transient stability. In addition, Fig. 20 implies that fixing κ_p and tuning κ_i, or tuning κ_p and κ_i simultaneously, can realize an equivalent design (the expected operating regime) to our implementation by fixing κ_i and tuning κ_p.

The consistency is supported by a further comparison of the sensitivity-based design guidelines given in Section V-B with the bifurcation diagram shown in Fig. 20(b). The specific bifurcations embodied by the design guidelines are summarized in Table VII. Hence, the qualitative difference in the design guidelines of the analysis methods can be interpreted by their different capability to capture the bifurcation behavior of grid-connected converters. Specifically, EAC and the energy function of the swing equation offer less effective parameter recommendations because they cannot capture the upper homoclinic bifurcation of the GFLC.

The consistency between TDS and bifurcation analysis is also found in the GFMC. Fig. 21 shows the sensitivity of t_c computed by TDS and the bifurcation diagram of the GFMC. The parameter range suggested by the sensitivity analysis overlaps with the expected operating regime given by bifurcation analysis, i.e., the bottom-right side of the homoclinic bifurcation. As the only crucial bifurcation of the GFMC, the homoclinic bifurcation is not captured by energy-based methods.

Overall, the comparison results indicate a varying consistency between the design guidelines of bifurcation analysis and other analysis methods. The reason is that the changes in sensitivity patterns, which serve as the criterion for identifying design guidelines, can be induced by the bifurcation behavior of grid-connected converters. Some stability analysis methods may only partially capture these crucial bifurcations, reflecting their limit in guiding design. This observation may provide important insights into the qualitative improvement of the stability analysis methods.

TABLE VIII
SENSITIVITY OF GFLC

κ_p (p.u.)	$\frac{\partial \Delta\theta_s}{\partial \kappa_p}$ (rad/p.u.)	$\frac{\partial \Delta\theta_s}{\partial L_s}$ (rad/p.u.)
0.01	282.74	−42.41
0.1	9.42	−6.28
0.25	0	0

TABLE IX
SENSITIVITY OF GFMC

ω_p (p.u.)	$\frac{\partial t_c}{\partial \omega_p}$ (s/p.u.)	$\frac{\partial t_c}{\partial L_l}$ (s/p.u.)
0.1	−1.4	−1.5
0.7	0	0

D. Robustness of Design

In addition, the consistency between sensitivity analysis and bifurcation analysis implies the advantage of sensitivity-based design guidelines in terms of the robustness of the design against parameter variations. For example, we present the sensitivity of a GFLC's critical phase jump to κ_p and L_s in Table VIII. Despite their relative difference, $\frac{\partial \Delta\theta_s}{\partial \kappa_p}$ and $\frac{\partial \Delta\theta_s}{\partial L_s}$ exhibit high, relatively high, and zero values simultaneously with $\kappa_p =$ 0.01, 0.1, 0.25 p.u., respectively. The three parameter settings correspond to the three phase portraits in Fig. 9 (one with quantitative difference for visualization), which primarily determine the overall consistent sensitivity patterns (high or low). For the recommended case with $\kappa_p = 0.25$ p.u., the GFLC works at the expected operating regime of bifurcation analysis, where the BOA boundary gets connected in line $y_\omega = 0$ and enables zero sensitivity to all parameters. We provide another example of a GFMC's critical clearing time against voltage dips in Table IX, where the consistency between $\frac{\partial t_c}{\partial \omega_p}$ and $\frac{\partial t_c}{\partial L_l}$ can be explained by the phase portraits in Fig. 10. These results demonstrate that while the main focus of sensitivity analysis in this work is to improve transient stability metrics, this approach can also benefit the robustness of the design against variations of uncontrollable parameters.

E. Requirement-Based Design Guidelines

While sensitivity-based design guidelines seek to exploit the optimal (suboptimal) robustness of grid-connected converters, requirement-based design guidelines aim to achieve a lower bound in performance. This lower bound is often manually set based on engineering experience. For instance, Chen et al. [19] proposed to meet the requirement of IEEE Standards 1547-2018 and developed an analytical condition using an improved Lyapunov function. Specifically, the requirement can be interpreted as the need for the GFMC to remain stable during a sustained voltage dip with $V_{sm}^f = 0.5$ p.u.

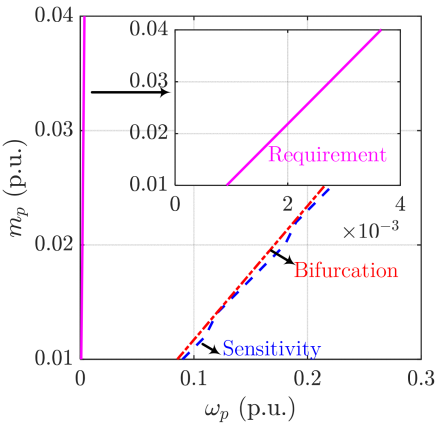

Fig. 22. Boundaries of design guidelines for GFMC derived by sensitivity analysis (TDS), bifurcation analysis, and setting requirement (Lyapunov method [19]), all with $L_l = 0.271$ p.u.

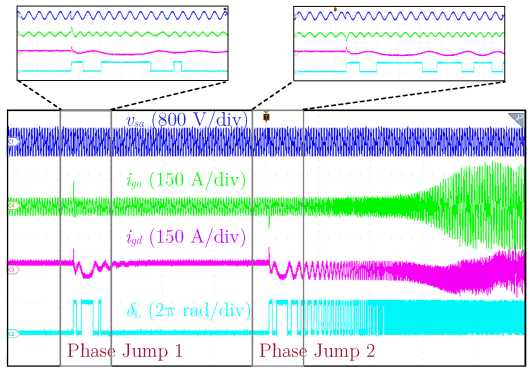

Time Scale: 400 ms/div

Fig. 23. Experimental waveforms of GFLC with $\kappa_p = 0.1$ p.u. suffering from phase jumps of 0.8π and 0.84π.

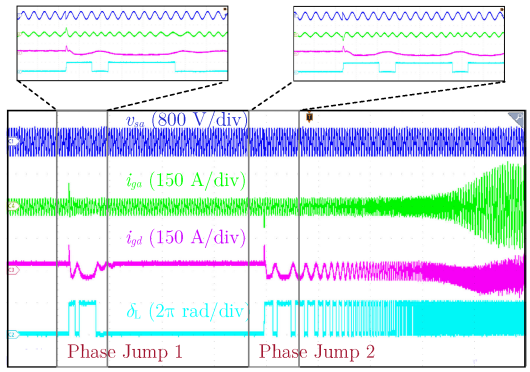

Time Scale: 400 ms/div

Fig. 24. Experimental waveforms of GFLC with $\kappa_p = 0.16$ p.u. suffering from phase jumps of 1.06π and 1.1π.

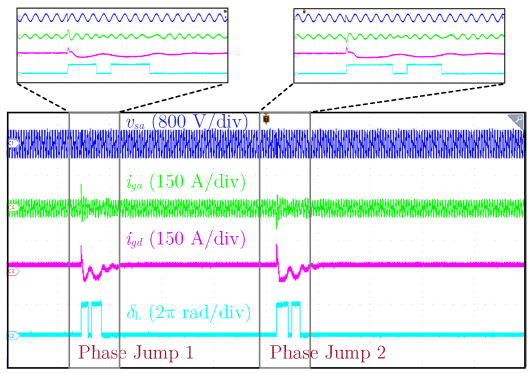

Time Scale: 400 ms/div

Fig. 25. Experimental waveforms of GFLC with $\kappa_p = 0.17$ p.u. suffering from phase jumps of 1.09π and 1.13π.

We compare their requirement-based design guidelines with our sensitivity-based design guidelines to show their values for practical design. The boundaries of the design guidelines are presented in Fig. 22, where the grid inductance L_l is reduced to 0.271 p.u. to allow for the presence of an equilibrium point during the fault. The analytical condition by Chen et al. [19] implies a linear relationship between ω_p and m_p on the design boundary. However, as shown in Fig. 22, the slope of the requirement-based design boundary is very large in our example, leading to extremely small ω_p for typical values of m_p. The comparison given in Fig. 22 indicates that the parameter range of the requirement-based design guidelines can be too broad to provide useful information. On the other hand, when the requirement is set too stringent (e.g., the condition by Chen et al. [19] under the default high-impedance scenario given in Table II), there may not exist a feasible solution. Therefore, applying the requirement-based design guidelines faces the same problem as applying the monotonic relationships, i.e., the dependence on engineering experience. In comparison, the sensitivity-based design guidelines offer better performance and facilitate the consideration of the impact of parameter variations. For these reasons, the parameter suggestions of the requirement-based method may serve as an initial solution and can be further verified by the sensitivity-based method.

VI. Experimental Verification

Control hardware-in-loop experiments are employed to verify the identified sensitivity patterns of stability metrics. Specifically, GFLCs and GFMCs with varying control parameters are tested with grid disturbances to demonstrate the changes of sensitivity patterns. The default parameters given in Tables I and II are adopted, unless otherwise stated. The converters and power grid are emulated using OPAL-RT OP4512, and the control signals are generated by DSP TMS320F28377D.

As summarized in Section V-B, the GFLC exhibits three sensitivity patterns of the critical phase jump $\Delta\theta_s$. Two of them are exposed by the responses of the GFLC with varying κ_p against phase jumps, as shown in Figs. 23–25. Judging from the convergence and divergence of post-fault waveforms, we obtain the critical phase jumps of the GFLC at $\kappa_p = 0.1$ p.u. and 0.16 p.u. as 0.82π and 1.08π, respectively. Thus, the sensitivity of $\Delta\theta_s$ to κ_p between the two cases is $13.6\,\mathrm{rad/p.u.}$, which is very close to the sensitivity estimates of

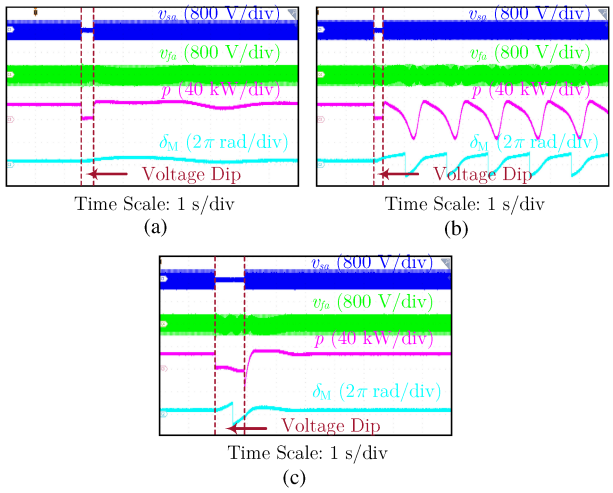

Fig. 26. Experimental waveforms of GFMC suffering from a voltage dip with $V_{sm}^f = 0.1$ p.u. (a) $\omega_p = 0.1$ p.u. the fault lasts for 0.4 s; (b) $\omega_p = 0.6$ p.u. the fault lasts for 0.3 s; (c) $\omega_p = 0.7$ p.u. the fault lasts for 1 s.

TDS and SOSP, as shown in Fig. 14(b). Furthermore, for a GFLC with $\kappa_p = 0.17$ p.u., which meets the design guidelines of TDS and bifurcation analysis (close to that of SOSP), we steer the converter's state to the two sides of the UEP by applying phase jumps of 1.09π and 1.13π. The waveforms given in Fig. 25 show the successful resynchronization of the GFLC, implying the connection of the SEP's BOA in line $y_\omega = 0$. As a result, the GFLC becomes robust to any phase jumps, confirming the zero-sensitivity range predicted by TDS, SOSP, and bifurcation analysis. Therefore, the experimental results of GFLCs verify the presence of the qualitatively different sensitivity patterns. In terms of design guidance, the results demonstrate a stronger robustness realized by following the design guidelines of TDS, SOSP, and bifurcation analysis.

As for the GFMC, the identified two sensitivity patterns of the critical clearing time t_c are verified by the experimental waveforms shown in Fig. 26. With a relatively low cutoff frequency $\omega_p = 0.1$ p.u., the GFMC resynchronizes after a voltage dip of 0.4 s. As ω_p increases to 0.6 p.u., the GFMC loses stability for a voltage dip of 0.3 s. The comparison between Fig. 26(a) and (b) indicates a negative sensitivity of t_c to ω_p between the two cases, which is consistent with the sensitivity estimates of all considered transient stability analysis methods, as shown in Fig. 18(b). However, a further increase of ω_p to 0.7 p.u., which meets the design guidelines of TDS and bifurcation analysis, enables the GFMC to survive a voltage dip of 1s, as shown in Fig. 26(c). Instead of continuing to decrease, t_c increases to a huge value (infinity in theory) due to the increase of ω_p beyond 0.67 p.u. Such an infinite t_c also signifies a zero sensitivity as predicted by TDS. This abrupt qualitative change in transient stability is captured by TDS and bifurcation analysis, indicating the effectiveness of design-oriented analysis.

VII. Conclusion

Despite their quantitative differences, the various methods for analyzing transient stability can identify similar sensitivity patterns of stability metrics, leading to equivalent parameter recommendations. We demonstrate this phenomenon in typical analysis methods for grid-following and GFMCs. Our results have multiple implications for design-oriented transient stability analysis.

1) *Sensitivity-based design guidelines:* Sensitivity analysis can identify the qualitative change in the dynamics of grid-connected converters, providing an informative approach to guide the control design. Besides, compared with requirement-based design guidelines, sensitivity-based design guidelines show better adaptability to different parameter conditions.
2) *Basis of sensitivity patterns:* The change in the sensitivity patterns of stability metrics, as captured by various analysis methods, can be induced by the bifurcation behavior of grid-connected converters. Hence, without delving into complex dynamics, engineers can exploit the conclusions from bifurcation analysis to confirm their design results derived from sensitivity analysis. Moreover, we can find clues of crucial changes of stability status from the design guidelines derived from other methods.
3) *Energy-based methods:* While algorithmic construction of Lyapunov functions gives less conservative results, the estimated BOA in the vertical axis (y_ω or $\Delta\omega_M$) is still limited by the presence of an UEP for grid-connected converters. As a result, the energy-based methods only partially capture the salient bifurcations (changes in stability status) of grid-connected converters. To overcome this limit, future work may omit the unstable equilibrium by adjusting the problem formulation.

References

[1] X. Wang, M. G. Taul, H. Wu, Y. Liao, F. Blaabjerg, and L. Harnefors, "Grid-synchronization stability of converter-based resources–An overview," *IEEE Open J. Ind. Appl.*, vol. 1, pp. 115–134, Aug. 2020.
[2] Joint NERC and Texas RE Staff Report, "Odessa disturbance," NERC, Atlanta, GA, USA, Tech. Rep., pp. 11–12, Sep. 2021. [Online]. Available: www.nerc.com
[3] C. K. Tse, M. Huang, X. Zhang, D. Liu, and X. L. Li, "Circuits and systems issues in power electronics penetrated power grid," *IEEE Open J. Circuits Syst.*, vol. 1, pp. 140–156, Sep. 2020.
[4] C. K. Tse and M. Li, "Design-oriented bifurcation analysis of power electronics systems," *Int. J. Bifurcation Chaos*, vol. 21, no. 06, pp. 1523–1537, 2011.
[5] D. Dong, B. Wen, D. Boroyevich, P. Mattavelli, and Y. Xue, "Analysis of phase-locked loop low-frequency stability in three-phase grid-connected power converters considering impedance interactions," *IEEE Trans. Ind. Electron.*, vol. 62, no. 1, pp. 310–321, Jan. 2015.
[6] H. Wu and X. Wang, "Design-oriented transient stability analysis of grid-connected converters with power synchronization control," *IEEE Trans. Ind. Electron.*, vol. 66, no. 8, pp. 6473–6482, Aug. 2019.
[7] D. Pan, X. Wang, F. Liu, and R. Shi, "Transient stability of voltage-source converters with grid-forming control: A design-oriented study," *IEEE J. Emerg. Sel. Topics Power Electron.*, vol. 8, no. 2, pp. 1019–1033, Jun. 2020.
[8] C. C. Liu, J. Yang, C. K. Tse, and M. Huang, "Transient synchronization stability of grid-following converters considering nonideal current loop," *IEEE Trans. Power Electron.*, vol. 38, no. 11, pp. 13757–13769, Nov. 2023.
[9] R. Ma et al., "Dominant transient equations of grid-following and grid-forming converters by controlling-unstable-equilibrium-point-based participation factor analysis," *IEEE Trans. Power Syst.*, vol. 39, no. 3, pp. 4818–4834, May 2024.

[10] H. Wu and X. Wang, "Design-oriented transient stability analysis of PLL-synchronized voltage-source converters," *IEEE Trans. Power Electron.*, vol. 35, no. 4, pp. 3573–3589, Apr. 2020.
[11] P. Kundur, *Power System Stability and Control*, 1st ed. New York, NY, USA: McGraw-Hill, 1994.
[12] Q. Hu, L. Fu, F. Ma, and F. Ji, "Large signal synchronizing instability of PLL-based VSC connected to weak AC grid," *IEEE Trans. Power Syst.*, vol. 34, no. 4, pp. 3220–3229, Jul. 2019.
[13] X. He, H. Geng, J. Xi, and J. M. Guerrero, "Resynchronization analysis and improvement of grid-connected VSCs during grid faults," *IEEE J. Emerg. Sel. Top. Power Electron.*, vol. 9, no. 1, pp. 438–450, Feb. 2021.
[14] R. Ma, J. Li, J. Kurths, S. Cheng, and M. Zhan, "Generalized swing equation and transient synchronous stability with PLL-based VSC," *IEEE Trans. Energy Convers.*, vol. 37, no. 2, pp. 1428–1441, Jun. 2022.
[15] X. Li et al., "Transient stability analysis for grid-tied VSG considering high-order nonlinear interactions between active and reactive power control loops," *IEEE Trans. Power Electron.*, vol. 39, no. 6, pp. 6974–6988, Jun. 2024.
[16] Z. Shuai, C. Shen, X. Liu, Z. Li, and Z. J. Shen, "Transient angle stability of virtual synchronous generators using Lyapunov's direct method," *IEEE Trans. Smart Grid*, vol. 10, no. 4, pp. 4648–4661, Jul. 2019.
[17] X. Fu et al., "Large-signal stability of grid-forming and grid-following controls in voltage source converter: A comparative study," *IEEE Trans. Power Electron.*, vol. 36, no. 7, pp. 7832–7840, Jul. 2021.
[18] C. Zhang, M. Molinas, Z. Li, and X. Cai, "Synchronizing stability analysis and region of attraction estimation of grid-feeding VSCs using sum-of-squares programming," *Front. Energy Res.*, vol. 8, 2020, Art. no. 56.
[19] S. Chen, Y. Sun, X. Hou, H. Han, S. Fu, and M. Su, "Quantitative parameters design of VSG oriented to transient synchronization stability," *IEEE Trans. Power Syst.*, vol. 38, no. 5, pp. 4978–4981, Sep. 2023.
[20] A. Abate, D. Ahmed, M. Giacobbe, and A. Peruffo, "Formal synthesis of Lyapunov neural networks," *IEEE Control Syst. Lett.*, vol. 5, no. 3, pp. 773–778, Jul. 2021.
[21] J. Yang, C. K. Tse, M. Huang, and X. Fu, "Homoclinic bifurcation of a grid-forming voltage source converter," *IEEE Trans. Power Electron.*, vol. 36, no. 11, pp. 13176–13187, Nov. 2021.
[22] J. Yang, C. K. Tse, M. Huang, D. Liu, C. C. Liu, and X. Fu, "Comparison of homoclinic bifurcations between grid-following and grid-forming converters," *IEEE Trans. Ind. Electron.*, vol. 71, no. 5, pp. 4731–4741, May 2024.
[23] M. Carreño, J. Song, O. Gomis-Bellmunt, and R. Griñó, "Design-oriented large-signal stability analysis of synchronous reference frame phase-locked loop," *IEEE Trans. Power Del.*, early access, Sep. 4, 2024, doi: 10.1109/TPWRD.2024.3454533.
[24] H.-D. Chiang, M. W. Hirsch, and F. F. Wu, "Stability regions of nonlinear autonomous dynamical systems," *IEEE Trans. Autom. Control*, vol. 33, no. 1, pp. 16–27, Jan. 1988.
[25] H. Wu and X. Wang, "Control of grid-forming VSCs: A perspective of adaptive fast/slow internal voltage source," *IEEE Trans. Power Electron.*, vol. 38, no. 8, pp. 10151–10169, Aug. 2023.
[26] S. Sharma, S. Pushpak, V. Chinde, and I. Dobson, "Sensitivity of transient stability critical clearing time," *IEEE Trans. Power Syst.*, vol. 33, no. 6, pp. 6476–6486, Nov. 2018.
[27] G. F. Franklin, J. D. Powell, and A. Emami-Naeini, *Feedback Control of Dynamic Systems*, 8th ed. Harlow, U.K.: Pearson, 2020.
[28] Y. A. Kuznetsov, *Elements of Applied Bifurcation Theory*, 2nd ed. New York, NY, USA: Springer, 1998.
[29] M. Lu, "Virtual oscillator grid-forming inverters: State of the art, modeling, and stability," *IEEE Trans. Power Electron.*, vol. 37, no. 10, pp. 11579–11591, Oct. 2022.
[30] P. A. Parrilo, *Structured Semidefinite Programs and Semialgebraic Geometry Methods in Robustness and Optimization*. Pasadena, CA, USA: California Inst. Technol., 2000.
[31] M. Anghel, F. Milano, and A. Papachristodoulou, "Algorithmic construction of Lyapunov functions for power system stability analysis," *IEEE Trans. Circuits Syst. I*, vol. 60, no. 9, pp. 2533–2546, Sep. 2013.
[32] A. Papachristodoulou et al., "SOSTOOLS: Sum of squares optimization toolbox for MATLAB," 2021, *arXiv:1310.4716*. [Online]. Available: https://github.com/oxfordcontrol/SOSTOOLS
[33] A. Abate, D. Ahmed, A. Edwards, M. Giacobbe, and A. Peruffo, "FOSSIL: A software tool for the formal synthesis of Lyapunov functions and barrier certificates using neural networks," in *Proc. HSCC '21*. ACM, May 2021, pp. 1–11.
[34] Z. Shuai, Y. Peng, X. Liu, Z. Li, J. M. Guerrero, and Z. J. Shen, "Parameter stability region analysis of islanded microgrid based on bifurcation theory," *IEEE Trans. Smart Grid*, vol. 10, no. 6, pp. 6580–6591, Nov. 2019.

Chao Charles Liu (Graduate Student Member, IEEE) received the B.S. and M.S. degrees in electrical engineering from Wuhan University, Wuhan, China, in 2018 and 2021, respectively. He is currently working toward the Ph.D. degree in electrical engineering with the Department of Electrical Engineering, City University of Hong Kong, Hong Kong.

His research interests include transient stability of grid-connected converters, applications of nonlinear dynamics, and smart meter data analytics.

Chi K. Tse (Fellow, IEEE) received the B.Eng. (Hons.) degree with first class honors and the Ph.D. degree from the University of Melbourne, Melbourne, VIC, Australia, in 1987 and 1991, respectively, both in electrical engineering.

He is currently an Associate Vice President (Innovation), the Chair Professor of electrical engineering, and the Director of Academy of Innovation, City University of Hong Kong, Hong Kong. His research interests include power electronics, nonlinear systems, and complex network applications.

Dr. Tse was the recipient of a number of research and invention prizes including the IEEE CASS Charles A. Desoer Technical Achievement Award in 2022 and a few Best Paper Prizes from IEEE and other journals, as well as Gold Medal with Jury's Commendations and Grand Prizes in International Exhibition of Inventions of Geneva 2024, Asia Exhibition of Innovations and Inventions 2023, and Silicon Valley International Invention Festival 2019. He has been appointed to honorary professorship and distinguished fellowship by a few Australian, Canadian, and Chinese universities, including the Chang Jiang Scholar Chair Professor with the Huazhong University of Science and Technology, Wuhan, China, the Honorary Professor of Melbourne University, and Distinguished Professor-at-Large with the University of Western Australia, Perth, WA, Australia. He also served as Panel Member of Hong Kong Research Grants Council, and Member of several professional and government committees. In 2005, 2010, and 2018, he was selected as an IEEE Distinguished Lecturer. In 2006, he chaired the IEEE CAS Technical Committee on Nonlinear Circuits and Systems. He serves and has served as the Editor-in-Chief for IEEE TRANSACTIONS ON CIRCUITS AND SYSTEMS II (2016–2019), IEEE Circuits and Systems Magazine (2013–2016), IEICE Nonlinear Theory and Applications (since 2013); as an Associate Editor for few other IEEE journals; and on the Editorial Board of IEEE Proceedings (2021–2024). He has served on a number of IEEE committees including the IEEE Fellows Committee and the IEEE Awards Committee, and chaired the Steering Committee for IEEE TRANSACTIONS ON NETWORK SCIENCE AND ENGINEERING.

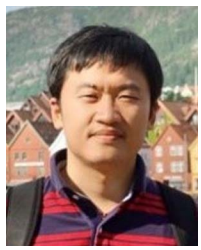

Meng Huang (Member, IEEE) received the B.Eng. and M.Eng. degrees in electronic science and technology from the Huazhong University of Science and Technology, Wuhan, China, in 2006 and 2008, respectively, and the Ph.D. degree in electronic and information engineering from the Hong Kong Polytechnic University, Hong Kong, in 2013.

He is currently a Professor with the School of Electrical Engineering and Automation, Wuhan University, Wuhan, China. His research interests include safe operation and control of grid-connected systems.

Dr. Huang was the recipient of the Best Paper Award of IEEE TRANSACTIONS ON POWER ELECTRONICS in 2016. He serves as the Editor for the *International Journal of Circuit Theory and Applications*, and was as Guest Editor for IEEE JOURNAL OF EMERGING AND SELECTED TOPICS OF CIRCUITS AND SYSTEMS, Guest Associate Editor for IEEE TRANSACTIONS ON INDUSTRIAL APPLICATIONS and IEEE JOURNAL OF EMERGING AND SELECTED TOPICS OF POWER ELECTRONICS.

Zhenxi Wu (Student Member, IEEE) received the B.S. degree in electronic engineering and automation from Central South University, Changsha, China, in 2020. She is currently working toward the joint Ph.D. degree in electrical engineering with the City University of Hong Kong, Hong Kong, and Central South University.

Her research interests include the stability analysis of power systems and microgrids.

Hua Han (Member, IEEE) received the M.S. and Ph.D. degrees in control science and engineering from the School of Automation, Central South University, Changsha, China, in 1998 and 2008, respectively.

She is currently a Professor with the School of Automation, Central South University. From 2011 to 2012, she was a Visiting Scholar with the University of Central Florida, Orlando, FL, USA. Her research interests include microgrids, renewable energy power generation systems, and power electronic equipment.

Jingxi Yang (Member, IEEE) received the B.S. and Ph.D. degrees in electrical engineering from Beijing Jiaotong University, Beijing, China, in 2014 and 2020, respectively.

He was a Postdoc, and is currently a Research Associate with the Department of Electrical Engineering, City University of Hong Kong, Hong Kong. His research interests include the complex nonlinear behavior and stability of grid-connected power electronic converter systems.

Dr. Yang was the recipient of the Excellent Reviewer Award of the *Journal of Modern Power Systems and Clean Energy* in 2022, and the Outstanding Reviewer Award of IEEE TRANSACTIONS ON POWER ELECTRONICS in 2021.